Macromolecules

pubs.acs.org/Macromolecules Article

Design and Synthesis of Colorless Cyclic Olefin Polymers with High Refractive Index, Transparency, and Thermal Stability

Weizhong Li, Yingli Ding, Huan Gao, Li Pan,* and Yuesheng Li*

Cite This: *Macromolecules* 2025, 58, 9459−9468 Read Online

ACCESS | Metrics & More | Article Recommendations | Supporting Information

ABSTRACT: High-refractive-index polymers are critical materials for optical applications. Cyclic olefin polymers (COPs) are among the most promising optical materials, but achieving high refractive indexes remains challenging. In this study, a series of high-refractive-index COPs was synthesized via ring-opening metathesis polymerization and subsequent hydrogenation, using three carbazole-based monomers (HM1−HM3), with HM2 and HM3 featuring naphthalene-fused structures. The resulting polymers exhibited high refractive indices (up to 1.697), Abbe numbers of 14.5−25.2, superior optical transparency (>90%), excellent thermal and processing stability (glass transition temperature: 140−180 °C; $T_{d5\%}$ > 400 °C), and low water absorption (<0.01%). Density functional theory (DFT) calculations and X-ray diffraction (XRD) analysis revealed that both molecular polarizability and chain packing contribute to the enhancement of refractive index. This study first incorporates carbazole−naphthalene-fused units into high-refractive-index polymers, offering a novel design strategy for optical materials.

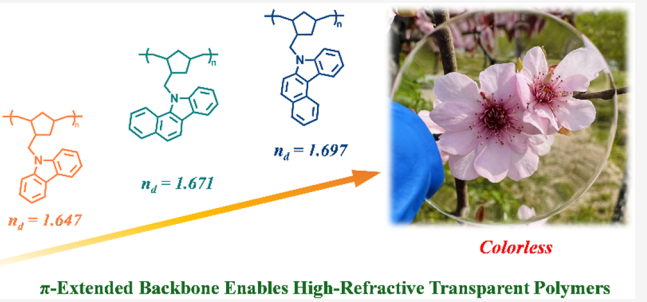

INTRODUCTION

High-refractive-index optical polymer materials are vital for advanced photonic systems, including under-display imaging, integrated optical circuits, and next-generation display panels.[1−5] Compared with inorganic glasses and metal oxides, organic polymers are easier to process, lighter, and more flexible.[6−9] Among them, cyclic olefin polymers (COPs) are seen as very promising because they exhibit high optical transmittance, high thermal stability, low optical dispersion, and low birefringence.[10−14] However, commercial COPs have aliphatic hydrocarbon backbones, which generally contribute to low refractive indices (<1.55), making it hard for them to meet the needs of high-performance optical parts that require a high refractive index (>1.60 or even >1.70).[15,16]

To enhance the refractive index (n) of polymeric materials, researchers often use molecular design strategies via incorporation of high-polarizability groups based on the Lorentz−Lorenz theory,[17] which correlates the refractive index with molecular polarizability. One effective strategy is to introduce strongly polarizable structural units, such as aromatic rings,[18−29] sulfur-containing groups,[30−39] or halogenated substituents,[40−42] into the polymer backbone or side chains. Specifically, representative rigid planar aromatic groups include fluorene,[18−21] carbazole,[23−26] and naphthalene,[27−29] which are widely employed to enhance the refractive index, owing to their strong π-electron delocalization and large electron cloud volumes. They contribute considerably to enhancing molecular polarizability, causing the refractive index of the resulting polymers to rise. The rational incorporation of these structural units offers an effective route for the design of high-refractive-index optical polymers.

As illustrated in Scheme 1, research on high-refractive-index COPs remains limited, with only two representative strategies reported to date.[16,19] One approach (Scheme 1a) incorporates fluorene-based aromatic monomers into a ROMP system, followed by hydrogenation. The resulting polymers exhibit refractive indices ranging from 1.576 to 1.615 and show excellent thermal stability, with glass transition temperatures (T_g) reaching up to 273 °C.[19] However, the optical transparency of this system was not reported, and the refractive index enhancement remained moderate. The second strategy (Scheme 1b) employs monomers bearing carbazole and indole moieties and enhances the refractive index primarily through the incorporation of the external 1,2-ethanedithiol (EDT) via UV-induced thiol−ene crosslinking. P1 refers to the copolymer derived from a ROMP copolymerization of equivalent amounts of a carbazole-based monomer and a dicyclopentadiene. The refractive index increases from 1.595 (without additives) to 1.684, mainly due to the introduction of a high sulfur content (25.25 wt %) in the resulting polymer networks.[16] Despite the

Received: June 11, 2025
Revised: July 26, 2025
Accepted: August 18, 2025
Published: August 22, 2025

https://doi.org/10.1021/acs.macromol.5c01567
Macromolecules 2025, 58, 9459−9468

Scheme 1. Comparison of Design Strategies for High-Refractive-Index COPs: (a) Fluorene-Based ROMP and Hydrogenation; (b) External Additive (EDT)-Assisted UV Crosslinking; (c) This Work Employs Carbazole-Fused Naphthalene Structures, Achieving a Maximum Refractive Index of 1.697 without Additives, along with Excellent Transparency, Thermal Stability, and Processability

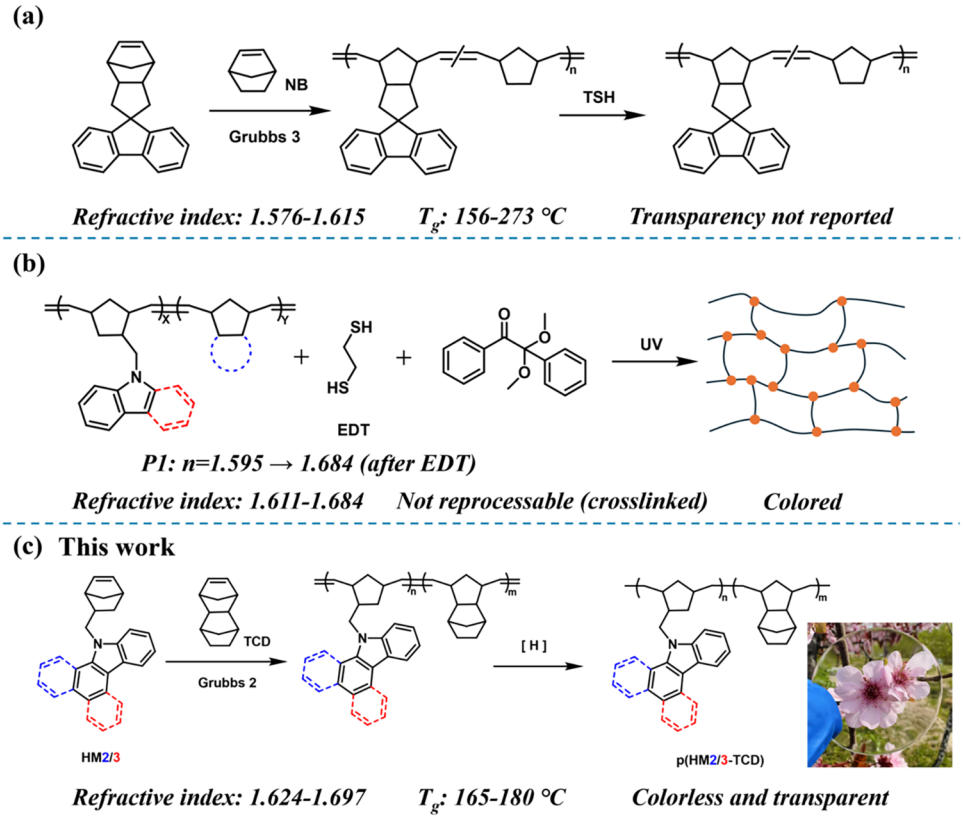

Scheme 2. Representation of the Synthetic Route and Chemical Structures of High-Refractive-Index COPs

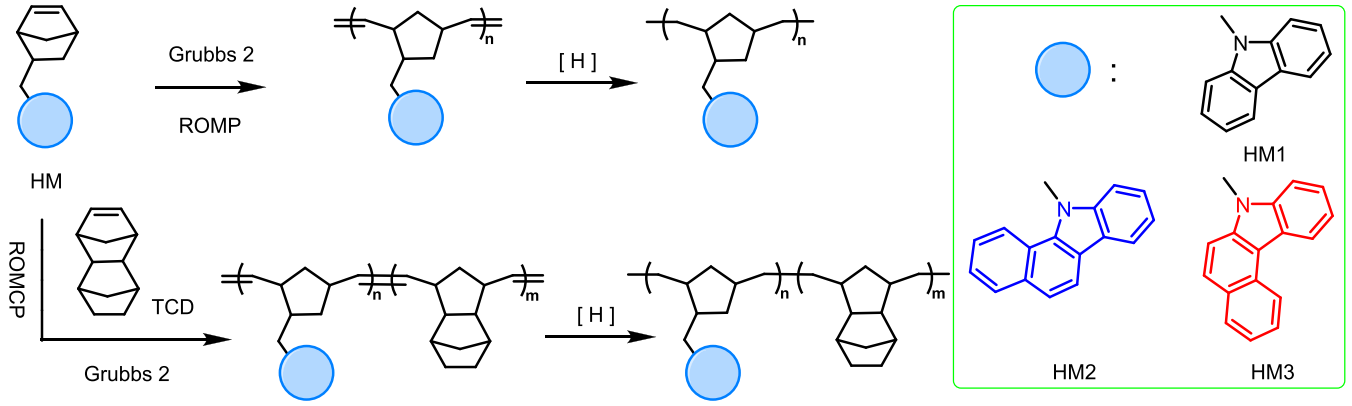

enhanced refractive index, the formation of the sulfur-based network inevitably causes inherent yellowish/brownish coloration and renders the material infusible and insoluble, limiting its fabrication methods. These limitations underscore the urgent need for novel COPs that simultaneously achieve a high refractive index, excellent transparency, a colorless appearance, and good processability for advanced optical applications.

As shown in Scheme 1c, to overcome these limitations, this study proposes a novel design strategy based on a carbazole framework with the help of density functional theory (DFT) calculation, incorporating naphthalene-fused structures to enhance molecular polarizability while preserving colorless transparency. For clarity, only representative high-refractive-index systems (based on HM2 and HM3) are shown in Scheme 1c, while the full data for HM1 and HM3 are discussed in the text. Unlike previously reported systems, the synthesized polymers exhibit refractive indices as high as 1.697, along with excellent optical clarity, colorless, good processability, and excellent thermal stability. Importantly, the remarkably high refractive indices were achieved purely through rational molecular design, without relying on external high-index additives.

RESULTS AND DISCUSSION

Design and Synthesis of HM-Based Polymers. High-refractive-index COPs were synthesized via ROMP catalyzed

https://doi.org/10.1021/acs.macromol.5c01567
Macromolecules 2025, 58, 9459−9468

Table 1. Results of HM and TCD Copolymerization[a]

entry	[HM]/[TCD]	yield (wt %)	HM incorp.[b] (mol %)	HM incorp.[b] (wt %)	T_g[c] (°C)	M_n[d] (10^4)	$Đ$[d]
1	HM1/–	99	100	100	140	7.40	1.58
2	HM1/TCD (4:1)	99	80	87	142	6.84	1.58
3	HM1/TCD (3:1)	99	75	84	143	6.83	1.61
4	HM1/TCD (2:1)	99	67	77	143	7.10	1.57
5	HM1/TCD (1:1)	99	50	63	145	6.99	1.59
6	HM2/–	99	100	100	180	8.07	1.55
7	HM2/TCD (4:1)	99	80	89	177	7.35	1.50
8	HM2/TCD (3:1)	99	75	86	176	7.06	1.49
9	HM2/TCD (2:1)	99	67	80	175	6.28	1.46
10	HM2/TCD (1:1)	99	50	67	172	6.35	1.61
11	HM3/–	99	100	100	174	8.78	1.52
12	HM3/TCD (4:1)	99	80	89	170	8.62	1.64
13	HM3/TCD (3:1)	99	75	86	169	8.53	1.66
14	HM3/TCD (2:1)	99	67	80	168	8.60	1.72
15	HM3/TCD (1:1)	99	50	67	165	8.13	1.74

[a]Polymerization conditions: Polymerization was performed using HM and TCD (total mass = 2.0 g) at a monomer-to-catalyst molar ratio of 400 in chlorobenzene (total volume = 30 mL) at room temperature for 2 h. [b]The HM content in the polymer (mol % and wt %) was determined by ^{1}H NMR spectroscopy. [c]Glass transition temperatures (T_g) were measured by differential scanning calorimetry (DSC). [d]Number-average molar mass (M_n) and polydispersity index ($Đ$) were determined by high-temperature gel permeation chromatography (GPC) in trichlorobenzene, using polystyrene (PS) standards for calibration. The listed data (T_g, M_n, $Đ$) correspond to the hydrogenated polymers.

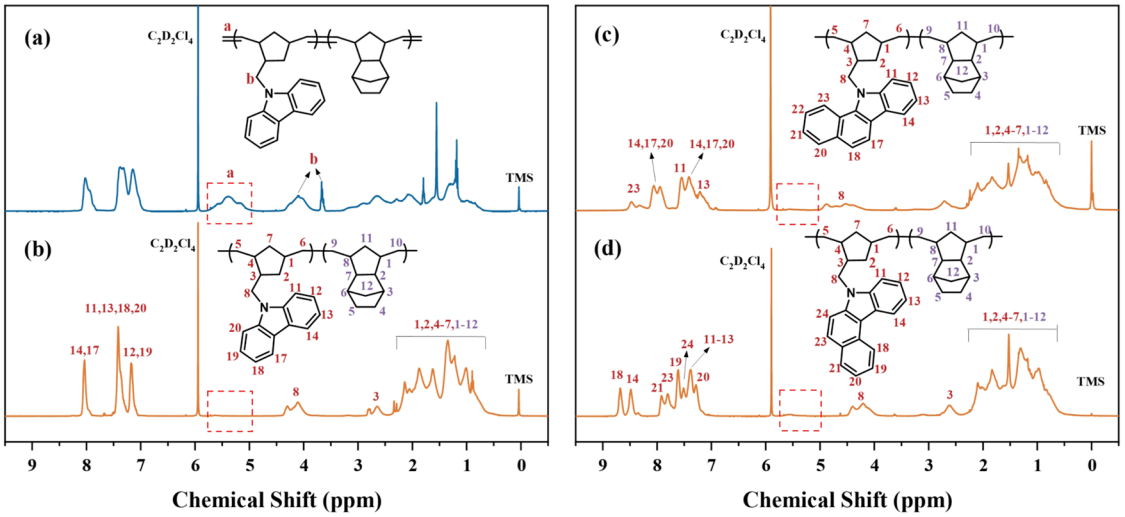

Figure 1. ^{1}H NMR spectra of the polymers: (a) p(HM1-TCD) (entry 5) before hydrogenation, (b) p(HM1-TCD) (entry 5) after hydrogenation, (c) hydrogenated polymer p(HM2-TCD) (entry 10), and (d) hydrogenated polymer p(HM3-TCD) (entry 15). Characteristic signals of aromatic and aliphatic protons are assigned.

by Grubbs' second-generation catalyst (G2), followed by hydrogenation to eliminate residual unsaturation and enhance stability.[10,13] As shown in Scheme 2, three monomers, HM1, HM2, and HM3, were designed based on a carbazole core, with HM2 and HM3 incorporating additional fused naphthalene rings to extend π-conjugation and enhance molecular polarizability. In addition to homopolymer synthesis, a comonomer, tetracyclo [6.2.1.1(3,6).0(2,7)]dodec-4-ene (TCD) was introduced to prepare a series of copolymers. The incorporation of bulky TCD enables modulation of the optical, thermal, and mechanical properties of the resulting polymers by adjusting the feed ratio.

For homopolymer synthesis, monomers HM1 and HM3 were polymerized in chlorobenzene at room temperature for 2 h at a monomer-to-catalyst ratio of 400. To improve thermal stability, the resulting polymers were subsequently hydrogenated using *p*-toluenesulfonyl hydrazide. For copolymer synthesis, HM1 and HM3 were copolymerized with TCD as a comonomer at various feed ratios (4:1, 3:1, 2:1, and 1:1) to achieve tunable optical and thermal properties. Copolymerizations were conducted under identical conditions to those for the homopolymerization, which was followed by subsequent hydrogenation. Polymerization conditions as well as resulting polymer composition are summarized in Table 1. All polymerizations exhibited almost complete monomer conversion with isolated yields up to 99%, highlighting the high efficiency of the ROMP process.

The number-average molar mass (M_n) and polydispersity index ($Đ$) of the prepared polymers were determined by gel permeation chromatography (GPC), as summarized in Table 1. For homopolymers, M_n ranged from 7.40 to 8.78 × 10^4 Da, with $Đ$ values between 1.52 and 1.58, which indicates a well-

https://doi.org/10.1021/acs.macromol.5c01567
Macromolecules 2025, 58, 9459−9468

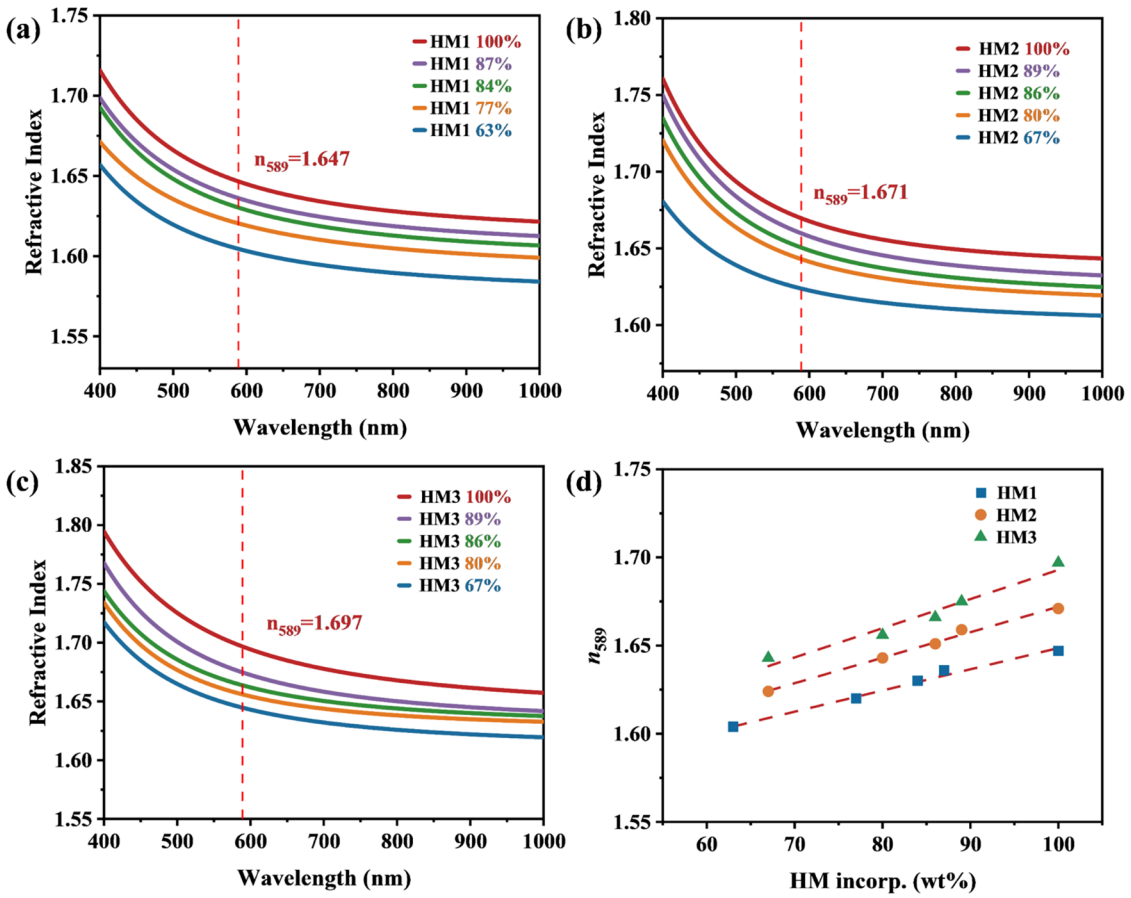

Figure 2. Refractive index characteristics of HM-based polymers. Wavelength-dependent refractive index curves of (a) HM1-based polymers with varying HM1 content. The red-dashed line indicates the refractive index at 589 nm, (b) HM2-based polymers with varying HM2 content, (c) HM3-based polymers with varying HM3 content, and (d) correlation between the refractive index at 589 nm (n_{589}) and HM incorporation (wt %) for HM-based polymers.

controlled polymerization process. Incorporation of TCD led to slight variations in M_n, with values ranging from 6.28 to 8.62 × 10^4 Da, depending on the HM/TCD feed ratio. The $Đ$ values remained within the range of 1.46−1.74, indicating a controlled polymerization process with narrow molar mass distributions.

As shown in Figure 1, the ^{1}H NMR spectra provide structural confirmation for both representative unsaturated and hydrogenated polymers. For p(HM1-TCD), olefinic proton signals presented in the 5−6 ppm region are clearly observed prior to hydrogenation (Figure 1a) but disappeared completely after hydrogenation (Figure 1b), confirming the full saturation of backbone double bonds. Similarly, for p(HM2-TCD) and p(HM3-TCD) (Figure 1c,1d), the disappearance of olefinic proton signals also confirms complete hydrogenation of the unsaturated main chains. Furthermore, the well-resolved aromatic and aliphatic proton signals in the ^{1}H NMR spectra confirm the successful incorporation of HM units and the structural integrity of the resulting polymers. Detailed ^{1}H and ^{13}C NMR spectra of HM monomers and corresponding polymers are provided in Figures S10−S24 in the Supporting Information. These spectral features validate the successful synthesis and postpolymerization modification of the high-refractive-index COPs.

Optical Properties of HM-Based Polymers. The refractive index, a key optical parameter, was systematically measured to investigate the structure−property relationships in the HM-based polymers. As shown in Figure 2a−c, the wavelength-dependent refractive index curves of p(HM1), p(HM2), and p(HM3) exhibit a consistent upward trend with increasing HM content, indicating that the highly polarizable carbazole and naphthalene-fused structures play a key role in enhancing refractive index. Among the homopolymers, p(HM3) exhibits the highest refractive index at 589 nm (n_{589} = 1.697), followed by p(HM2) (n_{589} = 1.671) and p(HM1) (n_{589} = 1.647). This trend persists throughout the full wavelength range of 400−1000 nm, confirming that molecular structure is a determining factor of the optical properties of these polymers. A clear positive correlation between the refractive index at 589 nm (n_{589}) and HM content is also observed (Figure 2d), indicating that increasing the incorporation of highly polarizable HM units effectively enhances the refractive index of the resulting polymers.

To gain deeper insight into the molecular origins of refractive index enhancement, density functional theory (DFT) calculations were performed on the repeat units of the synthesized homopolymers p(HM1), p(HM2), and p(HM3). Both the static polarizability (α_0) and the dynamic polarizability at 589 nm (α_{589}) were calculated for each structure. The relationship between refractive index and polarizability is described by the Lorentz−Lorenz equation[17]

$$\frac{n^2 - 1}{n^2 + 2} = \frac{4\pi}{3} N\alpha_m \quad (1)$$

https://doi.org/10.1021/acs.macromol.5c01567
Macromolecules 2025, 58, 9459−9468

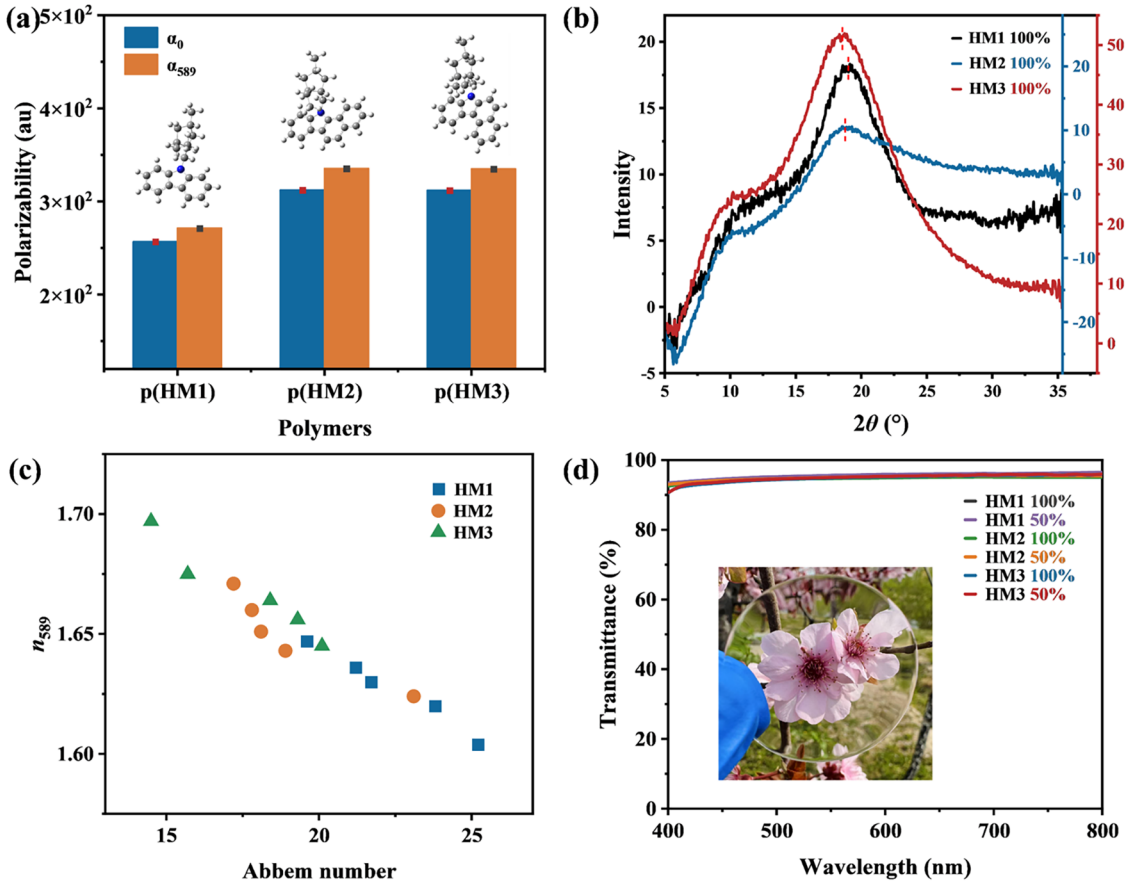

Figure 3. Optical, structural, and polarizability analyses of HM1-, HM2-, and HM3-based polymers. (a) Static polarizability (α_0) and dynamic polarizability at 589 nm (α_{589}) for p(HM1), p(HM2), and p(HM3) polymers. The molecular structures illustrate the optimized conformations used in polarizability calculations. (b) X-ray diffraction (XRD) patterns of p(HM1), p(HM2), and p(HM3) homopolymers, showing the influence of molecular packing on the polymer structure. (c) Correlation between the refractive index at 589 nm (n_{589}) and the Abbe number for HM1-, HM2-, and HM3-based polymers. (d) Optical transmittance of HM1-, HM2-, and HM3-based polymers with different HM incorporations, confirming high optical transparency in the visible range.

where n is the refractive index, N is the molecular number density, and α_m is the molecular polarizability. As shown in Figure 3a, Tables S1 and S2, both the static (α_0) and dynamic (α_{589}) polarizability values of p(HM2) and p(HM3) are nearly identical and significantly higher than those of p(HM1). This result suggests that the incorporation of naphtho-fused carbazole units effectively enhances molecular polarizability, leading to significantly higher refractive indices in p(HM2) and p(HM3) compared with p(HM1), thereby validating the molecular design strategy employed in this work. Although p(HM2) and p(HM3) exhibit similar polarizability values, the experimental refractive index of p(HM3) is noticeably higher (1.697 vs 1.671), suggesting that other factors beyond polarizability also contribute to the refractive index enhancement.

According to the Lorentz−Lorenz relationship, the refractive index is governed not only by molecular polarizability but also by the molecular number density (N). To further investigate the causes, the molecular packing behavior of the polymers was analyzed by X-ray diffraction (XRD). As shown in Figure 3b, all three polymers exhibit broad, diffuse scattering peaks, indicating predominantly amorphous structures. However, the intensity and sharpness of these peaks vary significantly. In particular, p(HM3) displays the sharpest and most intense peak, suggesting a more densely packed molecular arrangement. Denser packing implies a higher molecular number density, thereby increasing N and further enhancing the refractive index. To complement the XRD results, we further measured the densities of the homopolymers. As shown in Table S3, p(HM3) exhibits the highest density (1.282 g/cm^3), compared to p(HM2) (1.234 g/cm^3) and p(HM1) (1.138 g/cm^3), thereby confirming its tighter molecular packing. These results provide additional physical evidence supporting the conclusion that p(HM3) possesses denser molecular packing. Therefore, the superior refractive index of p(HM3) arises from the synergistic combination of a high molecular polarizability and dense molecular packing. This result highlights the synergistic effect of molecular polarizability and packing density on the refractive index enhancement in polymer systems.

Balancing the refractive index enhancement and chromatic dispersion control is an important consideration in the development of high-refractive-index polymers. The Abbe number (ν_d), which quantifies material dispersion, is inversely related to refractive index and is calculated as follows

$$\nu_d = \frac{n_d - 1}{n_F - n_C} \tag{2}$$

where n_d, n_F, and n_C denote the refractive indices at 589, 486, and 656 nm, respectively. A lower ν_d implies a higher

https://doi.org/10.1021/acs.macromol.5c01567
Macromolecules 2025, 58, 9459−9468

Table 2. Refractive Index (n) and Abbe Number (ν) of the Obtained Polymers

entry	polymers	HM incorp. (wt %)	n_d[a] (589 nm)	n_F[b] (486 nm)	n_C[c] (656 nm)	ν_d[d]
1	p(HM1)	100	1.647	1.671	1.638	19.6
2	p(HM1-TCD)	87	1.636	1.658	1.628	21.2
3	p(HM1-TCD)	84	1.630	1.651	1.622	21.7
4	p(HM1-TCD)	77	1.620	1.639	1.613	23.8
5	p(HM1-TCD)	63	1.604	1.622	1.598	25.2
6	p(HM2)	100	1.671	1.699	1.660	17.2
7	p(HM2-TCD)	89	1.660	1.689	1.652	17.8
8	p(HM2-TCD)	86	1.651	1.677	1.641	18.1
9	p(HM2-TCD)	80	1.643	1.669	1.635	18.9
10	p(HM2-TCD)	67	1.624	1.644	1.617	23.1
11	p(HM3)	100	1.697	1.732	1.684	14.5
12	p(HM3-TCD)	89	1.675	1.707	1.664	15.7
13	p(HM3-TCD)	86	1.664	1.691	1.655	18.4
14	p(HM3-TCD)	80	1.656	1.682	1.648	19.3
15	p(HM3-TCD)	67	1.645	1.669	1.637	20.1

[a]Refractive index at 589 nm. [b]Refractive index at 486 nm. [c]Refractive index at 656 nm. [d]Abbe number calculated using $\nu_d = (n_d - 1)/(n_F - n_C)$.

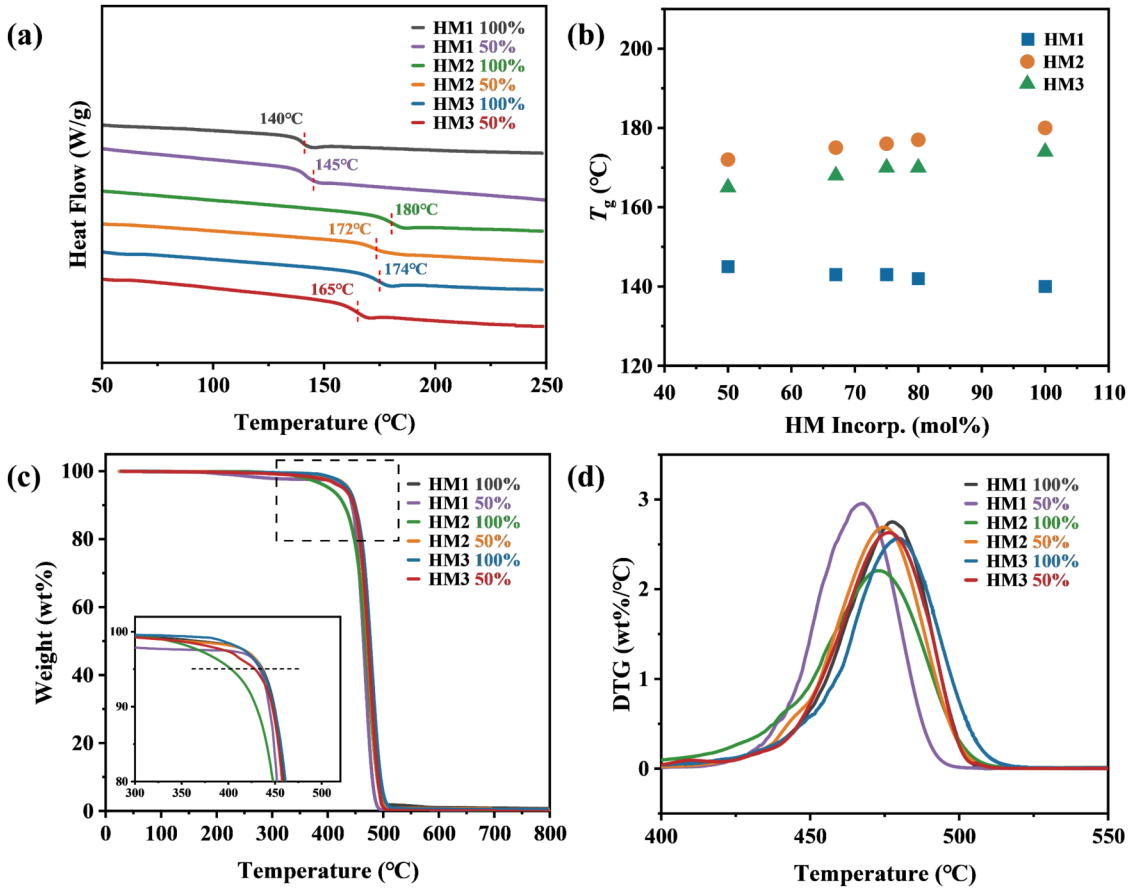

Figure 4. Thermal properties of HM-based polymers. (a) DSC curves showing the glass transition temperatures (T_g) of homopolymers and copolymers. (b) Glass transition temperature (T_g) as a function of HM incorporation (mol %) in the polymer backbone. (c) TGA curves of polymers with varying HM content. The inset highlights the decomposition behavior in the range of 300−525 °C. (d) DTG curves showing the rate of weight loss for each polymer composition.

chromatic dispersion, which is undesirable for typical applications of optical lenses. Among the homopolymers, p(HM3), with the highest refractive index (n_{589} = 1.697), possesses the lowest Abbe number (14.5), while p(HM1), with the lowest refractive index (n_{589} = 1.647) value, presents the largest ν_d (19.6). By copolymerizing with TCD, the refractive index and Abbe number can be tuned over a wide range (14.5−25.2), enabling compositional control of chromatic dispersion, while maintaining high refractive indices (1.604−1.697) across all polymers (Figure 3c and Table 2). Consequently, the synthesized polymers achieve a favorable balance between a high refractive index and controlled chromatic dispersion, making them promising candidates for advanced optical systems.

https://doi.org/10.1021/acs.macromol.5c01567
Macromolecules 2025, 58, 9459−9468

Table 3. Thermal Properties of the Obtained Polymers

entry	polymers	HM incorp. (mol %)	T_g (°C)	$T_{d5\%}$[a] (°C)	$T_{d10\%}$[b] (°C)	T_{max}[c] (°C)	ΔT[d] (°C)
1	p(HM1)	100	140	437	449	478	297
2	p(HM1-TCD)	80	142	440	453	477	298
3	p(HM1-TCD)	75	143	439	452	478	296
4	p(HM1-TCD)	67	143	444	454	478	301
5	p(HM1-TCD)	50	145	416	447	467	271
6	p(HM2)	100	180	403	430	473	223
7	p(HM2-TCD)	80	177	411	435	475	234
8	p(HM2-TCD)	75	176	418	437	474	242
9	p(HM2-TCD)	67	175	427	442	475	252
10	p(HM2-TCD)	50	172	436	447	475	264
11	p(HM3)	100	174	435	449	480	261
12	p(HM3-TCD)	80	170	432	448	479	262
13	p(HM3-TCD)	75	169	428	446	478	259
14	p(HM3-TCD)	67	168	418	438	475	250
15	p(HM3-TCD)	50	165	429	447	476	264

[a] $T_{d5\%}$ denotes the temperature at which 5% weight loss occurs, indicating the onset of thermal degradation. [b] $T_{d10\%}$ denotes the temperature at which 10% weight loss occurs, reflecting the material's thermal stability under more severe degradation conditions. [c] T_{max} values are derived from the peaks of the DTG curves for all HM-based polymers, indicating the temperature at which the maximum rate of thermal degradation occurs. [d] Thermal processing window ($\Delta T = T_{d5\%} - T_g$) of each polymer, illustrating the temperature gap between the onset of thermal degradation and the glass transition.

High-refractive-index polymers need excellent optical clarity to meet the demanding needs of advanced optics. As shown in the visible-light transmittance spectra (Figure 3d), all of the polymers exhibit transmittance values exceeding 90% in the range of 400−800 nm, demonstrating excellent transparency. The inset photo of Figure 3d corroborates this finding as well: a polymer film cast over a flower appears almost invisible under naked-eye inspection, showing the colorless and transparent character of the polymer. Achieving such a high transparency is particularly challenging for polymers containing aromatic and π-conjugated structures. In this work, naphtho-fused structures were incorporated into the carbazole backbone to achieve an effective extension of the π-conjugated system, thereby enhancing molecular polarizability while simultaneously suppressing absorption in the visible region. Through precise molecular design, the resulting polymers exhibit a combination of a high refractive index and excellent optical transparency, demonstrating great potential for advanced optical applications.

Thermal Properties of HM-Based Polymers. The thermal stability of high-refractive-index polymers is a critical factor influencing their performance in optical applications, especially under high-temperature conditions. To assess the thermal behavior of HM1-, HM2-, and HM3-based polymers, differential scanning calorimetry (DSC) and thermogravimetric analysis (TGA) were performed, as summarized in Figure 4 and Table 3. Illustrated by Figure 4a,4b, the three homopolymers' glass transition temperatures (T_g) are p(HM2) > p(HM3) > p(HM1), where the T_g of p(HM2) is the highest (180 °C) and the lowest for p(HM1) (140 °C). The reason for this trend is largely due to the differing degrees of side group rigidity. Compared with HM1, both HM2 and HM3 incorporate additional fused naphthalene rings on the carbazole core, which enhance π-conjugation and increase steric hindrance. These structural features limit the mobility of the polymer backbone segment and thus require higher thermal energy for initiating chain mobility.

The T_g values also have a strong dependence on the ratio of HM monomers incorporated into the copolymers. For HM2- and HM3-based copolymers, the higher the HM content, the more pronounced the T_g values are, consistent with the rigidifying role of the ring-fusion-structured aromatics. For the HM1-based copolymer system, on the other hand, there is a slight increase in T_g (140 −145 °C) as the content of HM1 decreased from 100 to 50%. This may be attributed to the bulky comonomer TCD being more rigid than HM1, facilitating tighter chain packing and slightly restricting molecular mobility, thereby resulting in a slight increase in T_g. For the HM2- and HM3-based systems, copolymerization generally leads to a decrease in the T_g. This is because TCD lowers the content of rigid aromatic units and increases polymer chain flexibility. Although TCD possesses a certain degree of rigidity, it remains lower than that of HM2 and HM3. As a result, its incorporation decreases the overall chain rigidity of the polymers and consequently lowers their T_g.

In addition to T_g, the thermal decomposition behavior of the HM-based polymers was systematically evaluated using thermogravimetric analysis (TGA). As shown in Figure 4c,4d, all of the polymers exhibited a single-step thermal degradation profile, which is typical for thermally stable organic materials and shows a uniform molecular structure. The small differences in the temperatures at which decomposition starts suggest that the polymers break down in a similar degradation mechanism, mainly through backbone breaking and the loss of aromatic parts. The $T_{d5\%}$ values of the homopolymers were between 403 and 437 °C. p(HM1) had the highest thermal stability, followed by p(HM3), and then p(HM2) with slightly lower stability. A similar trend was observed for $T_{d10\%}$, indicating consistent thermal stability across the polymer series. The superior thermal stability of p(HM1) and p(HM3) compared with p(HM2) may be attributed to more efficient molecular packing. In p(HM2), the less ordered aromatic structure may disturb $\pi-\pi$ stacking, making some weak points that break down earlier. All polymers exhibited $T_{d5\%}$ values above 400 °C and ΔT values exceeding 220 °C, indicating a broad thermal processing window suitable for versatile thermal shaping techniques such as compression molding. In addition, the high thermal stability of these

https://doi.org/10.1021/acs.macromol.5c01567
Macromolecules 2025, 58, 9459−9468

polymers supports high-temperature solution casting processes, while ensuring long-term dimensional and optical stability at high temperatures. These outstanding thermal properties demonstrate the great potential of HM-based polymers for advanced optical applications that demand both high-temperature resistance and excellent processability.

Wettability and Solubility of HM-Based Polymers. The wettability and solubility of HM-based COPs were systematically investigated as these properties directly influence the environmental stability and processing versatility of optical materials. All of the polymers exhibited excellent hydrophobicity, as evidenced by static water contact angles ranging from 103 to 105° (Table S4). This strong hydrophobicity is attributed to the nonpolar hydrogenated backbone and the incorporation of rigid aromatic side groups, such as carbazole and its fused-ring derivatives, which reduce surface energy and suppress polar interactions with water molecules. Among the samples, p(HM2) and p(HM3) exhibited the highest contact angles, likely due to their larger and more extended aromatic structures. All polymers exhibited extremely low water absorption (<0.01%), confirming their excellent resistance to moisture. These characteristics are critical for optical materials, as moisture uptake can compromise refractive index stability and mechanical integrity over time. The combination of a nonpolar backbone and rigid aromatic side groups contributes to the excellent water resistance of these polymers.

Solubility tests in various organic solvents (Table S4) showed that the polymers are highly soluble in halogenated solvents such as tetrachloroethane, chlorobenzene, and chloroform, facilitating solution processing and thin-film fabrication. This good solubility is attributed to the ability of halogenated solvents to effectively disrupt $\pi-\pi$ stacking interactions and solvate rigid aromatic polymer chains. In contrast, they exhibited limited or poor solubility in nonhalogenated aromatic solvents, such as toluene and xylene, primarily due to the rigid aromatic structures and strong intermolecular interactions. For a visual comparison, representative solubility photographs are provided in Figure S25. The combination of high hydrophobicity, low moisture absorption, and good solubility in certain solvents shows that HM-based polymers have great environmental durability and are easy to process. These features make them good choices for optical coatings, films, and devices that need to stay stable under humid conditions.

CONCLUSIONS

In summary, the incorporation of carbazole-based fused aromatic structures effectively overcomes the challenge of achieving a high refractive index while maintaining transparency and processability in COPs. The resulting polymers exhibited high refractive indices (n_{589} = 1.604−1.697), visible-light transmittance above 90%, and outstanding thermal and processing stability (T_g = 140−180 °C; $T_{d5\%}$ > 400 °C). These superior optical and thermal properties are attributed to both the incorporation of highly polarizable aromatic structures and their influence on polymer chain packing. Theoretical calculations and XRD analyses reveal that molecular polarizability and packing density synergistically contribute to refractive index enhancement. Notably, p(HM3) exhibited the highest refractive index, attributed to the combined effect of high molecular polarizability and dense molecular packing. This study presents an effective molecular design strategy for colorless, high-refractive-index, and thermally stable polymers toward next-generation optical materials.

ASSOCIATED CONTENT

Supporting Information

The Supporting Information is available free of charge at https://pubs.acs.org/doi/10.1021/acs.macromol.5c01567.

Experimental procedures, characterization data (NMR, DSC, TGA, and SEC), DFT calculations, and solubility tests (PDF)

AUTHOR INFORMATION

Corresponding Authors

Li Pan − *School of Materials Science and Engineering, State Key Laboratory of High-Performance Roll Materials and Composite Forming, Tianjin University, Tianjin 300350, China; Tianjin Key Laboratory of Composite and Functional Materials, Key Laboratory of Organic Integrated Circuits, Ministry of Education, Tianjin 300350, China;* orcid.org/0000-0002-9463-6856; Email: lilypan@tju.edu.cn

Yuesheng Li − *School of Materials Science and Engineering, State Key Laboratory of High-Performance Roll Materials and Composite Forming, Tianjin University, Tianjin 300350, China; Tianjin Key Laboratory of Composite and Functional Materials, Key Laboratory of Organic Integrated Circuits, Ministry of Education, Tianjin 300350, China;* orcid.org/0000-0003-4637-4254; Email: ysli@tju.edu.cn

Authors

Weizhong Li − *School of Materials Science and Engineering, State Key Laboratory of High-Performance Roll Materials and Composite Forming, Tianjin University, Tianjin 300350, China*

Yingli Ding − *Tianjin Key Laboratory of Composite and Functional Materials, Key Laboratory of Organic Integrated Circuits, Ministry of Education, Tianjin 300350, China*

Huan Gao − *School of Materials Science and Engineering, State Key Laboratory of High-Performance Roll Materials and Composite Forming, Tianjin University, Tianjin 300350, China*

Complete contact information is available at: https://pubs.acs.org/10.1021/acs.macromol.5c01567

Author Contributions

The manuscript was written through the contributions of all authors. All authors have given approval to the final version of the manuscript.

Notes

The authors declare no competing financial interest.

ACKNOWLEDGMENTS

The authors are grateful for financial support from the National Natural Key Research and Development Program of China (2023YFB3608800) and the National Natural Science Foundation of China (No. 52373013).

REFERENCES

(1) Badur, T.; Dams, C.; Hampp, N. High refractive index polymers by design. *Macromolecules* **2018**, *51* (11), 4220−4228.

(2) Higashihara, T.; Ueda, M. Recent progress in high refractive index polymers. *Macromolecules* **2015**, *48* (7), 1915−1929.

(3) Huo, N.; Tenhaeff, W. E. High refractive index polymer thin films by charge-transfer complexation. *Macromolecules* **2023**, *56* (5), 2113−2122.
(4) Lee, L.-H.; Chen, W.-C. High-refractive-index thin films prepared from trialkoxysilane-capped poly(methyl methacrylate)−titania materials. *Chem. Mater.* **2001**, *13* (3), 1137−1142.
(5) Okutsu, R.; Suzuki, Y.; Ando, S.; Ueda, M. Poly(thioether sulfone) with high refractive index and high Abbe's number. *Macromolecules* **2008**, *41* (16), 6165−6168.
(6) Khan, S.; Iqbal, A. Organic polymers revolution: Applications and formation strategies, and future perspectives. *J. Polym. Sci. Eng.* **2023**, *6* (1), 3125.
(7) Liu, K.; Ouyang, B.; Guo, X.; Guo, Y.; Liu, Y. Advances in flexible organic field-effect transistors and their applications for flexible electronics. *npj Flexible Electron.* **2022**, *6* (1), 1.
(8) Noh, J.; Jeong, S.; Lee, J.-Y. Ultrafast formation of air-processable and high-quality polymer films on an aqueous substrate. *Nat. Commun.* **2016**, *7* (1), No. 12374.
(9) Root, S. E.; Savagatrup, S.; Printz, A. D.; Rodriquez, D.; Lipomi, D. J. Mechanical properties of organic semiconductors for stretchable, highly flexible, and mechanically robust electronics. *Chem. Rev.* **2017**, *117* (9), 6467−6499.
(10) Cui, J.; Yang, J. X.; Pan, L.; Li, Y. S. Synthesis of Novel Cyclic Olefin Polymer with High Glass Transition Temperature via Ring-Opening Metathesis Polymerization. *Macromol. Chem. Phys.* **2016**, *217* (24), 2708−2716.
(11) Cui, J.; Yang, J.-X.; Li, Y.-G.; Li, Y.-S. Synthesis of high performance cyclic olefin polymers (COPs) with ester group via ring-opening metathesis polymerization. *Polymers* **2015**, *7* (8), 1389−1409.
(12) Yang, J. X.; Cui, J.; Long, Y. Y.; Li, Y. G.; Li, Y. S. Synthesis of novel cyclic olefin polymers with excellent transparency and high glass-transition temperature via gradient copolymerization of bulky cyclic olefin and cis-cyclooctene. *J. Polym. Sci., Part A: Polym. Chem.* **2014**, *52* (22), 3240−3249.
(13) Zhang, Y.; Guo, J.; Zhang, K.; Ma, X.; Cao, D.; Bai, S.; Yuan, X.; Pan, L.; Sun, J.; Li, Y. Robust ionic cyclic olefin polymers with excellent transparency, barrier properties, and antibacterial properties. *Macromolecules* **2023**, *56* (11), 4371−4385.
(14) Zhang, Y.-R.; Yang, J.-X.; Pan, L.; Li, Y.-S. Synthesis of high performance cyclic olefin polymers using highly efficient WCl 6-based catalyst system. *Chin. J. Polym. Sci.* **2018**, *36*, 214−221.
(15) Yuan, H.; Kida, T.; Ishitobi, Y.; Tanaka, R.; Yamaguchi, M.; Nakayama, Y.; Shiono, T. Cyclic olefin copolymer bearing pendant fluorenyl groups with high refractive index and low chromatic dispersion. *Macromolecules* **2022**, *55* (1), 125−132.
(16) Zhang, J.; Zhang, Y.; Cui, L.; Jian, Z. High-Refractive-Index Cross-Linked Cyclic Olefin Polymers with Excellent Transparency via Thiol−Ene Click Reaction. *ACS Macro Lett.* **2024**, *13* (6), 781−787.
(17) Kragh, H. The Lorenz-Lorentz formula: Origin and early history. *Substantia* **2018**, *2* (2), 7−18.
(18) Iino, S.; Sobu, S.; Nakabayashi, K.; Samitsu, S.; Mori, H. Highly transparent and photopatternable spirobifluorene-based polythioethers with high refractive indices via thiol-ene click chemistry. *Polymer* **2021**, *224*, No. 123725.
(19) Ishii, S.; Ota, Y.; Matsuoka, S.-i.; Suzuki, M. Spiro-fluorene-containing cyclic olefin polymers. *ACS Appl. Polym. Mater.* **2023**, *5* (9), 7614−7620.
(20) Macdonald, E. K.; Lacey, J. C.; Ogura, I.; Shaver, M. P. Aromatic polyphosphonates as high refractive index polymers. *Eur. Polym. J.* **2017**, *87*, 14−23.
(21) Nakabayashi, K.; Imai, T.; Fu, M.-C.; Ando, S.; Higashihara, T.; Ueda, M. Poly(phenylene thioether)s with fluorene-based cardo structure toward high transparency, high refractive index, and low birefringence. *Macromolecules* **2016**, *49* (16), 5849−5856.
(22) Nakagawa, Y.; Suzuki, Y.; Higashihara, T.; Ando, S.; Ueda, M. Synthesis of highly refractive poly(phenylene thioether)s containing a binaphthyl or diphenylfluorene unit. *Polym. Chem.* **2012**, *3* (9), 2531−2536.
(23) Davis, T. P.; Gallagher, M. J.; Ranasinghe, M. G.; Zammit, M. D. Synthesis of high refractive index acrylic copolymers. *J. Mater. Chem.* **1994**, *4* (9), 1359−1363.
(24) Dou, Z.; Li, J.; Shi, Z.; Sun, J.; Fang, Q. Carbazole-Based Optical Polymers with Both High Refractive Index and High Abbe Number. *ACS Appl. Polym. Mater.* **2025**, *7*, 5302−5311, DOI: 10.1021/acsapm.5c01023.
(25) McGrath, J. E.; Rasmussen, L.; Shultz, A. R.; Shobha, H.; Sankarapandian, M.; Glass, T.; Long, T. E.; Pasquale, A. J. Novel carbazole phenoxy-based methacrylates to produce high-refractive index polymers. *Polymer* **2006**, *47* (11), 4042−4057.
(26) Sakurada, T.; Tomita, R.; Takagi, K.; Ueki, S. Development of Photocurable Resins Exhibiting a High Refractive Index and Low Abbe Number for Optical Applications. *ACS Appl. Polym. Mater.* **2025**, *7* (5), 3318−3323.
(27) Briesenick, M.; Gallei, M.; Kickelbick, G. High-refractive-index polysiloxanes containing naphthyl and phenanthrenyl groups and their thermally cross-linked resins. *Macromolecules* **2022**, *55* (11), 4675−4691.
(28) Chen, S.; Chen, D.; Lu, M.; Zhang, X.; Li, H.; Zhang, X.; Yang, X.; Li, X.; Tu, Y.; Li, C. Y. Incorporating pendent fullerenes with high refractive index backbones: a conjunction effect method for high refractive index polymers. *Macromolecules* **2015**, *48* (23), 8480−8488.
(29) Wei, Q.; Pötzsch, R.; Liu, X.; Komber, H.; Kiriy, A.; Voit, B.; Will, P. A.; Lenk, S.; Reineke, S. Hyperbranched polymers with high transparency and inherent high refractive index for application in organic light-emitting diodes. *Adv. Funct. Mater.* **2016**, *26* (15), 2545−2553.
(30) Choi, K.; Jang, W.; Lee, W.; Choi, J. S.; Kang, M.; Kim, J.; Char, K.; Lim, J.; Im, S. G. Systematic control of sulfur chain length of high refractive index, transparent sulfur-containing polymers with enhanced thermal stability. *Macromolecules* **2022**, *55* (16), 7222−7231.
(31) Fang, L.; Sun, J.; Chen, X.; Tao, Y.; Zhou, J.; Wang, C.; Fang, Q. Phosphorus-and sulfur-containing high-refractive-index polymers with high T g and transparency derived from a bio-based aldehyde. *Macromolecules* **2020**, *53* (1), 125−131.
(32) Kim, D. H.; Jang, W.; Choi, K.; Choi, J. S.; Pyun, J.; Lim, J.; Char, K.; Im, S. G. One-step vapor-phase synthesis of transparent high refractive index sulfur-containing polymers. *Sci. Adv.* **2020**, *6* (28), No. eabb5320.
(33) Kim, H.; Ku, B.-C.; Goh, M.; Ko, H. C.; Ando, S.; You, N.-H. Synergistic effect of sulfur and chalcogen atoms on the enhanced refractive indices of polyimides in the visible and near-infrared regions. *Macromolecules* **2019**, *52* (3), 827−834.
(34) Kleine, T. S.; Nguyen, N. A.; Anderson, L. E.; Namnabat, S.; LaVilla, E. A.; Showghi, S. A.; Dirlam, P. T.; Arrington, C. B.; Manchester, M. S.; Schwiegerling, J.; et al. High refractive index copolymers with improved thermomechanical properties via the inverse vulcanization of sulfur and 1,3,5-triisopropenylbenzene. *ACS Macro Lett.* **2016**, *5* (10), 1152−1156.
(35) Mazumder, K.; Komber, H.; Bittrich, E.; Voit, B.; Banerjee, S. Sulfur containing high refractive index poly(arylene thioether)s and poly(arylene ether)s. *Macromolecules* **2022**, *55* (3), 1015−1029.
(36) Nishant, A.; Kim, K. J.; Showghi, S. A.; Himmelhuber, R.; Kleine, T. S.; Lee, T.; Pyun, J.; Norwood, R. A. High refractive index chalcogenide hybrid inorganic/organic polymers for integrated photonics. *Adv. Opt. Mater.* **2022**, *10* (16), No. 2200176.
(37) Okutsu, R.; Ando, S.; Ueda, M. Sulfur-containing poly(meth)-acrylates with high refractive indices and high Abbe's numbers. *Chem. Mater.* **2008**, *20* (12), 4017−4023.
(38) Sun, Z.; Huang, H.; Li, L.; Liu, L.; Chen, Y. Polythioamides of high refractive index by direct polymerization of aliphatic primary diamines in the presence of elemental sulfur. *Macromolecules* **2017**, *50* (21), 8505−8511.
(39) Wuliu, Y.; Huang, G.; Tan, J.; Dong, W.; Huang, H.; Mu, K.; Feng, L.; Wang, M.-g.; Tian, L.; Zhu, C.; Xu, J. High refractive index and high Abbe number polymer based on norbornadiene. *Macromolecules* **2023**, *56* (23), 9881−9887.

https://doi.org/10.1021/acs.macromol.5c01567
Macromolecules 2025, 58, 9459−9468

(40) Huo, N.; Rivkin, J.; Jia, R.; Zhao, Y.; Tenhaeff, W. E. Synthesis of High Refractive Index Polymer Thin Films for Soft, Flexible Optics Through Halomethane Quaternization of Poly(4-Vinylpyridine). *Adv. Opt. Mater.* **2024**, *12* (10), No. 2302201.
(41) Allcock, H. R.; Bender, J. D.; Chang, Y.; McKenzie, M.; Fone, M. M. Controlled refractive index polymers: polyphosphazenes with chlorinated-and fluorinated-, aryloxy-and alkoxy-side-groups. *Chem. Mater.* **2003**, *15* (2), 473−477.
(42) Kwon, S.; Bae, J.; Lee, I. Iodine insertion and dispersion of refractive index in organic single crystal semiconductor. *Sci. Rep.* **2018**, *8* (1), No. 3370.

https://doi.org/10.1021/acs.macromol.5c01567
Macromolecules 2025, 58, 9459−9468